Cortical and white matter T1w/T2w development proceed in concert during early infancy

Stephanie Zika[1,2*], Kelly Chang[3,4], Altan Orhon[3,4], John Kruper[3,4], Ariel Rokem[3,4], & Mareike Grotheer[1,2]

1. Department of Psychology, Philipps-Universität Marburg, Schulstraße 12, 35037 Marburg, Germany
2. Center for Mind, Brain and Behavior - CMBB, Universities of Marburg, Gießen, and Darmstadt, Germany
3. Department of Psychology, University of Washington, Seattle, WA 98105
4. eScience Institute, University of Washington, Seattle, WA 98105

Corresponding author*: zikast@staff.uni-marburg.de

Abstract (150 words)

The infant brain undergoes rapid myelin growth that is critical for healthy brain function. This development has been characterized for gray and white matter independently, but the link between gray and white matter myelination remains unexplored. To close this knowledge gap, we processed large-scale (N=279) Developing Human Connectome Project data with automated software to identify 26 white matter bundles and map their cortical terminations, before evaluating T1w/T2w development in individuals. We found that mean T1w/T2w as well as the slope of T1w/T2w development are correlated across tissues. This synchrony of brain T1w/T2w is impacted by birth age and postnatal experience, whereas inter-individual differences in this synchrony predict motor outcomes at 17 - 25 months of age. As T1w/T2w is associated with myelin content, our results reveal an intricate relationship between gray and white matter myelination, highlighting the importance of conjointly evaluating both tissues.

Introduction

The human brain shows rapid development during early life. At birth, total brain volume is about 35% of adult size, growing to nearly 80% by the age of two years old[1,] (for review see [2]). This remarkable expansion is accompanied by changes in tissue microstructure and organization, including growth of myelin in both gray and white matter[3–6] (for reviews see [7–9]). Myelination is a critical process in brain development that involves wrapping neuronal axons in a fatty sheath, thereby enabling rapid and synchronized neural communication. This mechanism is essential for brain plasticity and learning, and disruptions in myelin development have been linked to various developmental and cognitive disorders[10,11] (for reviews see [12–15]).

In the white matter, myelin insulates axons for rapid saltatory conduction, reduces the energetic cost of signaling by lowering membrane capacitance, supplies metabolic substrates, and preserves axonal structural integrity[16–18] (for reviews see[19,13]). Although the majority of myelin is located in the white matter[20,21], a considerable number of myelinated axons can also be found in the gray matter[22,23] (for review see[24–27]). The precise role of cortical myelin remains debated, with several functions proposed, including i) metabolic support[28], ii) network synchronization[29,30] (for review see[31]), iii) fine-tuning of conduction speed[32], and iv) growth inhibition to prevent aberrant axonal sprouting and synapse formation[33–36] (for review see[37]).

In both white and gray matter, myelination during early infancy follows a complex spatio-temporal trajectory and, critically, similar mechanisms have been proposed to describe these developmental trajectories across tissues: 1) Spatial gradients: In white matter, several spatial gradients of myelination have been proposed including increasing developmental rates from: peripheral-to-central[38–41], anterior-to-posterior[38,5] and inferior-to-superior[5,42–45] white matter locations. Similarly, in gray matter, studies revealed higher myelin content in primary sensorimotor areas, with a systematic decrease toward transmodal regions - particularly in parietal, temporal, and prefrontal cortices[4,22,46–50]. 2) Functional systems: Sensory and motor white matter pathways myelinate earlier than pathways associated with higher-level brain functions[38,41] (for review see[51]). Similarly, sensory and motor gray matter regions myelinate early and heavy, while higher-order areas such as the prefrontal and association cortices, myelinate later and remain more lightly myelinated even in adulthood[3,4,22,52–57] (for review see[58]). 3) Myelin content at birth: Recent neuroimaging work suggests that white matter that is less myelinated at birth develops more rapidly postnatally[3,59] (for review see[60]). Similarly, in gray matter, primary sensory and primary motor cortices, which exhibit higher myelin levels at term-equivalent age, myelinate more slowly than higher-order association and visual areas during early infancy[4,57,61] (for review see[62]). Importantly, these mechanisms are likely not mutually-exclusive but rather shape myelin development in concert. Moreover, as the mechanisms that control the spatiotemporal trajectory of myelination in gray and white matter show substantial overlap, there may be an as of yet unexplored link between gray and white matter myelination during infancy.

A central theory of myelin growth across the lifespan is the theory of activity-dependent myelination. This theory proposes that neural activity promotes myelin production, thereby leading to increased myelination of active connections. This, in turn, optimizes signal transmission across the brain and offers a capacity for learning, as differences in neural activity induced by training or lifetime experiences can directly impact myelination. This theory of activity-dependent myelination is based on rodent studies showing that neuronal activity can influence oligodendrocyte precursor cell (OPC) proliferation, differentiation, and the subsequent formation of myelin sheaths[63–65] (for review see[66]). For example, experiments have demonstrated that increased neuronal firing, often induced through environmental enrichment or specific learning tasks, leads to enhanced myelination in related brain regions[67–69] (for review see[70]). Critically, as neural activity would simultaneously promote myelination of a region's local (in gray matter) and long-range (in white matter) connections, the theory of experience-dependent myelination predicts that gray and white matter myelination are coupled during learning and development.

To test this prediction, it is critical to follow and compare the trajectories of myelin growth of gray and white matter in the living human brain. Recent advances in quantitative MRI[3,43,71–73] (for review see[74]), have made it feasible to quantify myelin levels and to compare them between individuals and across developmental timepoints. The validity of using qMRI measures such as the myelin-water-fraction (MWF) or the longitudinal relaxation rate (R1), to study myelin development has been confirmed by comparisons to post-mortem histological data[75–77]. However, qMRI measures often require long acquisition times, and such measures are hence typically not included in large-scale open data, including in the dataset leveraged here. As a practical alternative, Glasser and Van Essen[22] proposed utilizing the ratio of

T1-weighted (T1w) to T2-weighted (T2w) images. Although the validity of T1w/T2w as a marker of myelin remains debated[78–81], studies comparing T1w/T2w to R1 have validated its usability in adult cortex[82] and infant white matter[59]. As the T1w/T2w ratio is easily computed from commonly acquired images, it is particularly useful in large-scale data sets and/or early life samples where acquisition times are particularly restricted.

Here we tested for a potential link between gray and white matter myelination in early infancy by relating T1w/T2w values of white matter bundles to T1w/T2w measured at their corresponding cortical targets in large-scale infant data shared by the developing human connectome project (dHCP). We find that white matter and cortical myelin contents are tightly linked: T1w/T2w measured within each bundle was positively correlated with T1w/T2w measured at its corresponding cortical targets. The rate of change in T1w/T2w during early infancy was similarly coupled between white and gray matter. In measurements conducted shortly after birth, the coupling between T1w/T2w in white and gray matter is weaker at preterm than at full-term birth, yet infants born prematurely show higher coupling of T1w/T2w across tissues once they reach term-equivalent age. We also observed marked inter-individual variability in the strengths of white and gray matter T1w/T2w coupling, and individuals with higher correlations demonstrated superior motor performance on a standardized test administered between 17 and 25 months of age.

We propose that the observed link between gray and white matter myelination is most readily accounted for by the theory of activity-dependent myelination. By highlighting the tight coupling of gray and white matter myelin growths, our findings provide a comprehensive understanding of early life brain myelination and suggest that white and gray matter myelination should be considered conjointly, especially as their synchrony can explain inter-individual differences in behavioral outcomes.

Results

<u>T1w/T2w of white matter bundles correlates with T1w/T2w of their gray matter targets</u>

We assessed the link between T1w/T2w development in white matter bundles and their corresponding gray matter targets during early infancy. We used pyBabyAFQ to identify 26 white matter bundles in individual infants' brains, mapped their endpoints to cortex (Fig. 1), and then conjointly assessed the development of T1w/T2w in both tissues. We studied two partially overlapping samples from the dHCP data: i) the "cross-sectional sample", which contained 279 infants, including both preterm and full-term infants, scanned shortly after birth (gestational age (GA) at birth: range: 24.57 to 42.29 weeks, mean ± SD: 38.04 ± 3.73 weeks; time between birth and scan: range: 0 to 16.71 weeks, mean ± SD: 1.54 ± 2.21 weeks). ii) the "longitudinal sample", which contained a sample of 26 preterm infants (GA at birth: mean SD: 32.04 ± 2.97 weeks) scanned once shortly after birth (GA at first scan: mean SD: 34.33 ± 1.76 weeks) and once after they reached a GA of at least 37 weeks (GA at second scan: mean SD: 40.70 ± 1.08 weeks), as well as a group of full-term infants with scan ages and genders matched to the preterm infants second scan (GA at scan: mean SD: 40.93 ± 1.44 weeks).

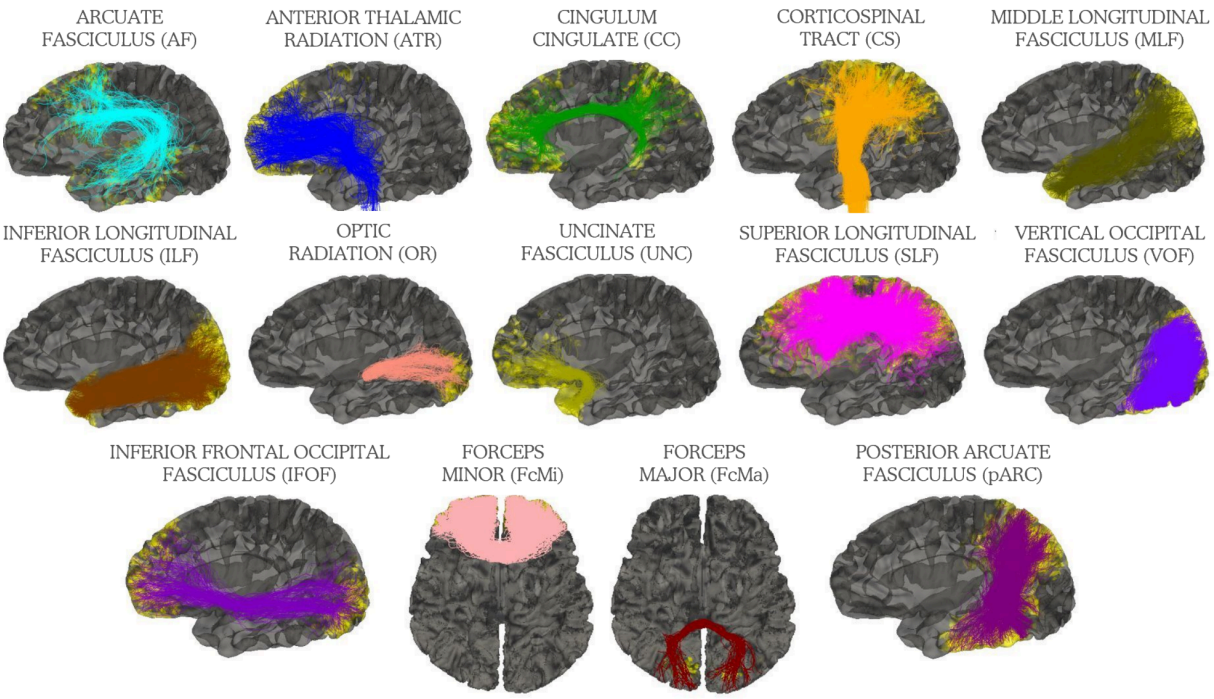

Figure 1. The bundles identified with pyBabyAFQ in the native brain space of one example infant scanned at 40 weeks after gestation. The yellow dots represent the cortical endpoints of the respective bundles. For bilateral bundles only the left hemisphere is shown.

To investigate the relationship between T1w/T2w of white and gray matter in early infancy, we started with the cross-sectional sample and correlated the mean T1w/T2w of the white matter bundles with the mean T1w/T2w of their gray matter targets. Our analysis revealed a positive correlation (Fig. 2A, $r^2 = 0.55$, p-value = $1.45e^{-5}$), indicating that if a white matter bundle has high T1w/T2w, its gray matter targets also have high T1w/T2w. This analysis also revealed interesting patterns among different bundles: The corticospinal tract (CS) and the optic radiation (OR) along with their cortical targets, showed particularly high T1w/T2w; in contrast, the posterior arcuate fasciculus (pARC) and its cortical targets exhibited comparatively low T1w/T2w, with other bundles showing intermediate values of T1w/T2w. In the ventral occipital fasciculus (VOF) and anterior thalamic radiation (ATR) the link between T1w/T2w in gray and white matter is less pronounced than in the other bundles, with the cortical targets of the ATR having lower T1w/T2w and the cortical targets of the VOF having higher T1w/T2w than expected based on their white matter T1w/T2w. Interestingly, our analysis also revealed similar T1w/T2w across hemispheres in gray and white matter of all bilateral bundles as indicated by the close proximity of data points representing corresponding bundles in each hemisphere.

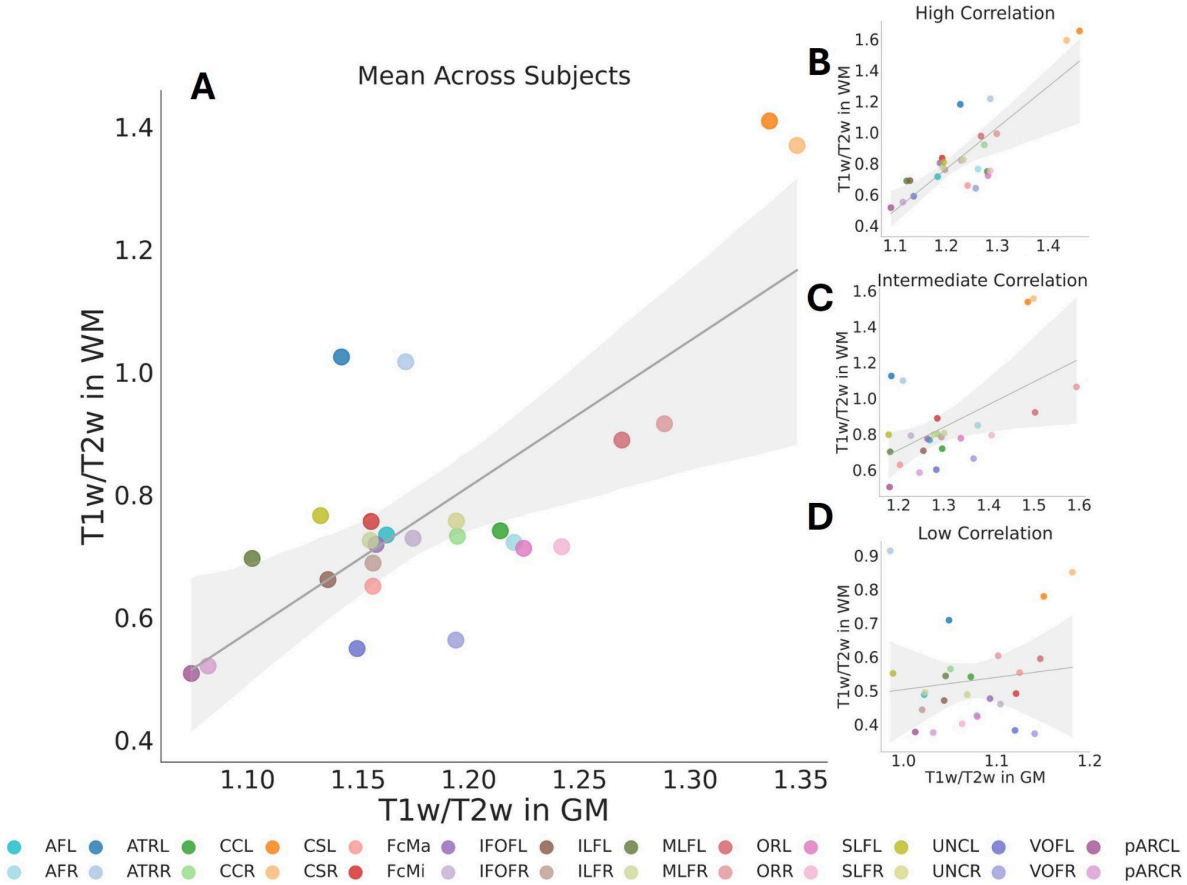

Figure 2. Relationship between T1w/T2w of white matter (WM) bundles and their respective gray matter (GM) targets. Each dot is a bundle. (A) Mean correlation with values averaged across all subjects (r^2=0.55, p-value=1.45e^{-5}). (B-D) Example individual subjects exhibiting high (B, r^2=0.68, p-value=2.28e^{-7}), intermediate (C, r^2=0.31, p-value= 0.003) and low (D, r^2=0.017, p-value=0.52) correlation between T1w/T2w of white and gray matter. The mean r^2 value for correlations computed within individuals is r^2=0.42. Abbreviations: AF: Arcuate Fasciculus, ATR: Anterior Thalamic Radiation], CC: Cingulum Cingulate, CS: Cortico-Spinal Tract, FcMa: Forceps Major, FcMi: Forceps Minor, IFO: Inferior Frontal Occipital Fasciculus, ILF: Inferior Longitudinal Fasciculus, MLF: Middle Longitudinal Fasciculus, OR: Optic Radiation, SLF: Superior Longitudinal Fasciculus, UNC: Uncinate Fasciculus, VOF: Ventral Occipital Fasciculus, pARC: Posterior Arcuate Fasciculus, L=left, R=right.

In addition to evaluating the relationship of the mean T1w/T2w of gray and white matter across all subjects, we also evaluated this relationship within each individual participant. These individual subjects analyses corroborated the group-level findings, as white and gray matter T1w/T2w were correlated within most individuals (correlation significant in 265 out of 273 subjects, mean r^2 across subjects: 0.42, mean p-value across subjects: p=0.008). Nonetheless, there were large inter-individual differences in the relationship of T1w/T2w in white and gray matter across subjects (range of r^2: 0.01-0.68, standard deviation of r^2: 0.13). Figure 2B-D shows three example individuals representing high (Fig. 2B; r^2=0.69, p<0.0001), medium (Fig. 2C, r^2=0.31, p=0.003) and low (Fig. 2D; r^2=0.014, p-value=0.52) correlations between T1w/T2w of white matter bundles and their cortical targets. Similar to the group level data, in the individual subject analyses the CS showed particularly high gray and white matter T1w/T2w and the pARC showed comparatively low T1w/T2w in gray and white matter, with other bundles falling in between. Further, again similar to the group-level data, the cortical targets of the ATR show lower T1w/T2w and the cortical targets of the VOF show higher

T1w/T2w than expected based on their white matter T1w/T2w. Finally, overall bilateral bundles show similar T1w/T2w in gray and white matter across hemispheres in the individual subject analyses as well.

The T1w/T2w coupling across tissues is linked to infant's motor skills later in life

The previous analysis showed considerable inter-individual differences in the strengths of the relationship between T1w/T2w of white and gray matter and we assessed whether these inter-individual differences have behavioral consequences. To do so, we analyzed a subset of infants from the cross-section sample (N=215) that also completed the Bayley-III questionnaire, and hence allowed us to link T1w/T2w measurements taken at birth to motor, cognitive, and language outcomes assessed between 17 and 25 months of age. For the three Bayley-III subscales (motor, language, and cognition) we investigated the relationship between each individual's standardized test scores and their correlation of T1w/T2w measured along white matter bundles and their cortical targets. For cognition and language, we found no significant link between the correlation of T1w/T2w in white and gray matter and performance (all $r^2<0.007$, all ps>0.11, Fig, 3A,B), however, we find that the correlation of T1w/T2w across tissues predicts later-life motor performance ($r^2=0.02$, p=0.015, significant with a Bonferroni corrected threshold, Figure 3C), suggesting that the coupling of gray and white matter T1w/T2w has behavioral consequences. We also tested if T1w/T2w measured in gray matter or in white matter alone is linked to later-life behavioral outcomes (Supplementary Figure S1), but found no significant relationship between T1w/T2w in either tissue and any of the three subscales (all $r^2<0.007$, all ps>0.23)

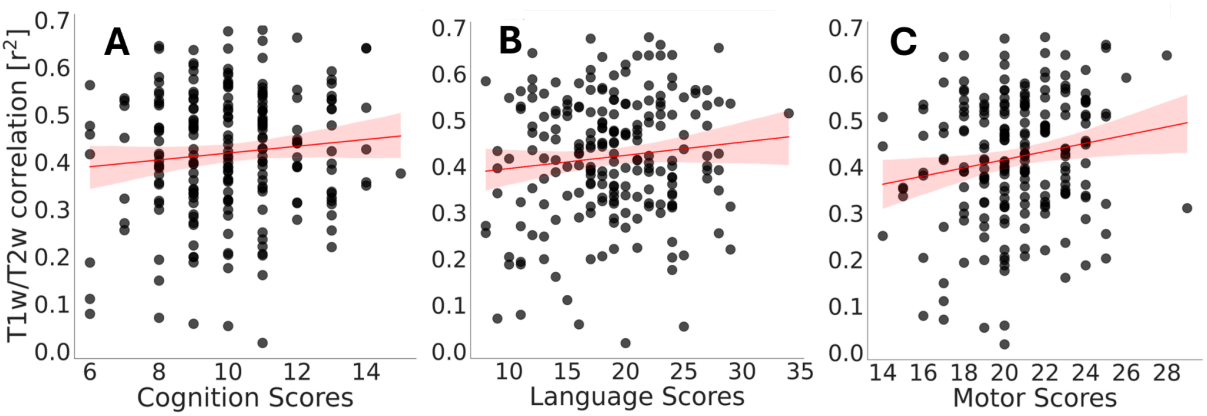

Figure 3: Relationship between behavioral performance and the correlation between T1w/T2w in gray and white matter. Relationship between the cognition (A; $r^2=0.01$, p-value=0.14), language (B; $r^2=0.01$, p-value=0.11) and motor (C; $r^2=0.03$, p-value=0.015) subscale of the Bayley-III and the correlation between T1w/T2w in gray and white matter in each individual subject. We found a significant relationship between an individual infant's motor ability and the correlation of T1w/T2w in gray and white matter, but not in any other subscale.

The slope of white and gray matter T1w/T2w growths is correlated during early infancy

We further investigated the relationship between T1w/T2w of white matter bundles and T1w/T2w of their cortical targets by analyzing the slopes of T1w/T2w growth (Fig. 4). These slopes represent the rate at which T1w/T2w increases relative to the infants' age in weeks at the time of measurement. Figure 4A-C shows the T1w/T2w growth in relation to age for three example white matter bundles: the corticospinal tract (CS, A), forceps minor (FcMi, B) and

inferior longitudinal fasciculus (ILF, C). Each data point represents an individual subject, a visualization of all bundles is provided in Supplementary Figure S2. All bundles showed a positive correlation between infants' age at measurement and T1w/T2w in both the white matter (all $r^2>0.47$, all $p<1.98e^{-39}$) and their cortical targets (all $r^2<0.39$, all $p<7.62e^{-31}$). While gray matter generally exhibited higher T1w/T2w compared to white matter, the slopes of T1w/T2w change were steeper in the white matter than the gray matter across bundles (t=3.82, p-value=0.0008). In fact, in the cortico-spinal tract, we observed a cross-over at around 37 where white matter T1w/T2w exceeded gray matter T1w/T2w. There was a stronger correlation between white matter T1w/T2w and infants' scan age compared to gray matter (mean delta in r^2 = 0.07, mean delta of AIC = 45.02).

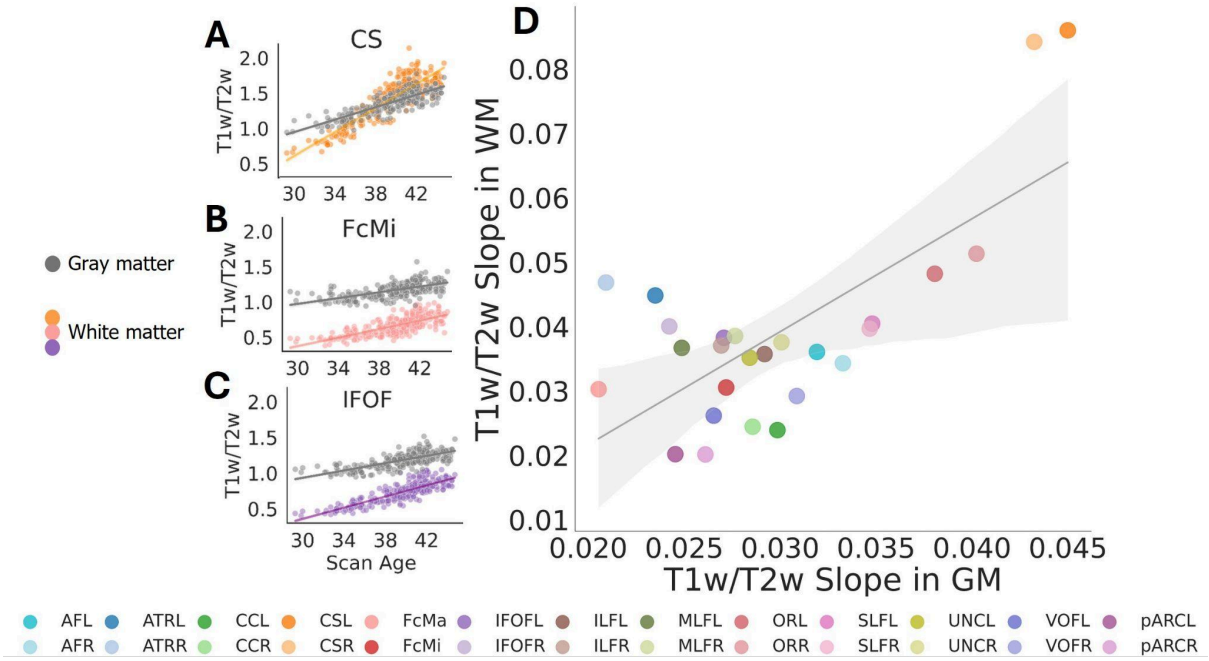

Figure 4: The rates of change of white and gray matter T1w/T2w are correlated across bundles. (A, B, C) Three example bundles illustrate how T1w/T2w slopes (rates of change) were computed by relating T1w/T2w to scan age in both gray and white matter. Gray circles indicate gray matter T1w/T2w in each subject, colored circles represent the white matter T1w/T2w in each subject, steepness of the lines indicate slope of T1w/T2w change with increasing age at measurement. For all bundles see Figure S2. (D) The slopes of T1w/T2w growth along white matter (WM) bundles and their gray matter (GM) targets are positively correlated (r^2=0.49, p-value=$7.57e^{-5}$). The slope indicates the increase in T1w/T2w values relative to the infants' age at the time of measurement in weeks, each dot is a bundle. Abbreviations: AF: Arcuate Fasciculus, ATR: Anterior Thalamic Radiation, CC: Cingulum Cingulate, CS: Cortico-Spinal Tract, FcMa: Forceps Major, FcMi: Forceps Minor, IFO: Inferior Frontal Occipital Fasciculus, ILF: Inferior Longitudinal Fasciculus, MLF: Middle Longitudinal Fasciculus, OR: Optic Radiation, SLF: Superior Longitudinal Fasciculus, UNC: Uncinate Fasciculus, VOF: Ventral Occipital Fasciculus, pARC: Posterior Arcuate Fasciculus, L=left, R=right.

Similar to the mean T1w/T2w values reported above, different bundles varied in the slopes of T1w/T2w change in gray and white matter. The CS, for instance, stood out with the highest rate of change in both the white matter and at its cortical target. In contrast, the pARC and the FcMi exhibit comparatively low rate of change, with the other bundles falling in between. Further, again similar to the mean T1w/T2w values, bilateral bundles showed similar gray and white matter slopes between the left and right hemisphere.

To determine if there is a relationship between the slope of white and gray matter T1w/T2w growth across bundles, we correlated T1w/T2w slopes of both tissues across bundles (Fig. 4D). This analysis revealed a positive correlation between the slopes of T1w/T2w of white matter bundles and their cortical targets (r^2=0.49, p<0.0001), suggesting a relationship of white and gray matter T1w/T2w development during early infancy.

<u>The correlation between gray and white matter T1w/T2w increases with infant development</u>

To examine if the relationship of T1w/T2w between white and gray matter depends on gestational age and/or prematurity, we compared this correlation between three groups from a small longitudinal sample (N=26): preterm infants scanned shortly after birth (Fig. 5A; r^2=0.43, p-value=0.0002), the same preterm infants scanned at term-equivalent age (Fig. 5B; r^2=0.54, p<0.0001), and full-term infants matched by age and gender to the preterm infants' second scan (Fig. 5C; r^2=0.53, p<0.0001). To determine whether the observed differences in correlation coefficients between groups were statistically significant, we employed a non-parametric bootstrap resampling procedure (1,000 iterations) to estimate the sampling distribution of each pairwise difference. The resulting 95% confidence intervals (CIs) were then compared against 0 to assess whether group differences were significant. This analysis revealed weaker correlation between T1w/T2w of white matter bundles and their cortical targets in the preterm infants at their first scan, compared to their full-term peers (Fig. 5D, mean difference in r^2=-0.07, 0 fell outside 95% CI [-0.075, -0.066]). Similarly, we also found weaker correlations within the preterm infants at their first compared to their second scan (Fig. 5E, mean difference in r^2 =-0.08 0 fell outside 95% CI [-0.082, -0.077]). Most interestingly, when we compared preterm infants at their second scan to their age-matched full-term peers, we found a slightly higher correlation in the preterm infants (Fig. 5F, mean difference in r^2=0.007, 0 fell outside 95% CI [0.004, 0.009]).

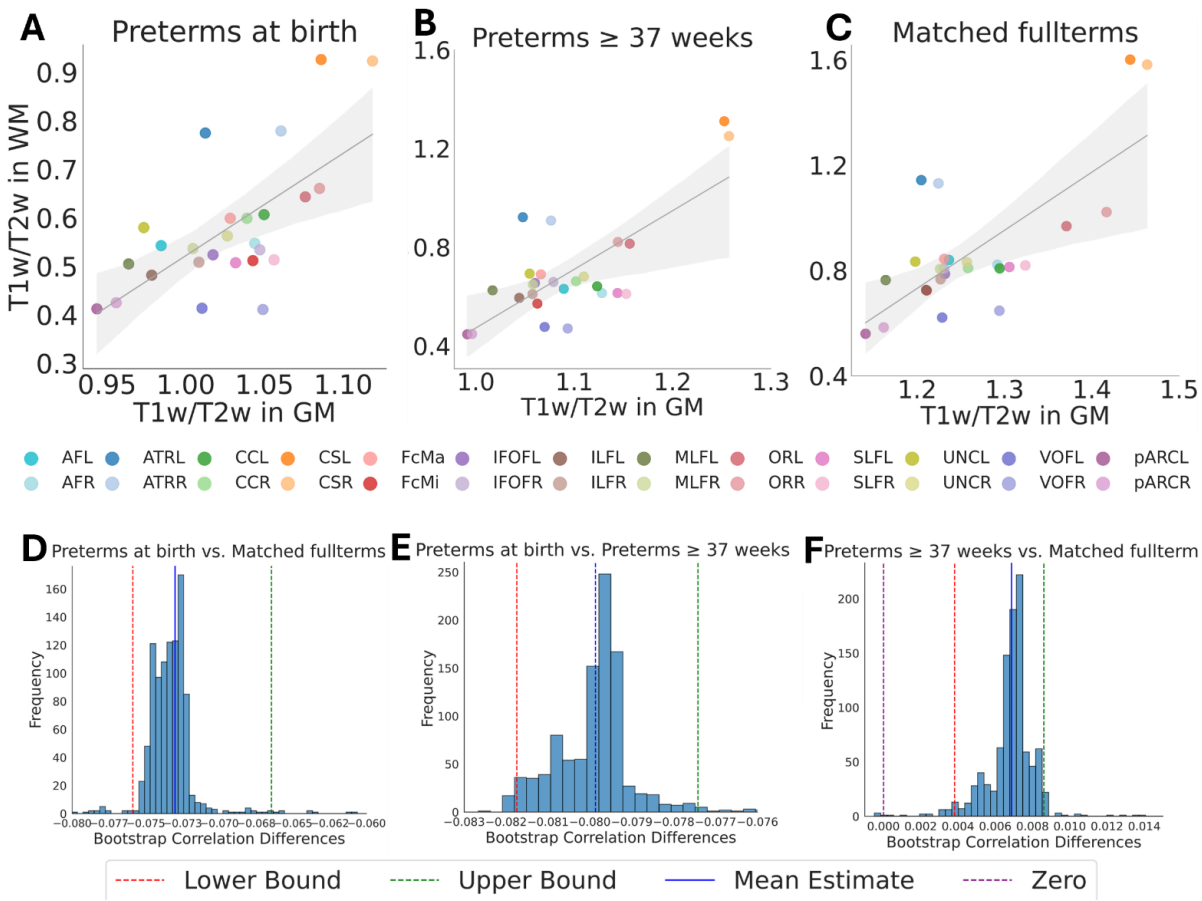

Figure 5: A-C: Relationship between T1w/T2w of white matter (WM) bundles and their respective gray matter (GM) targets in three groups: A: infants born preterm scanned at birth (r^2=0.43, p-value=0.0002); B: infants born preterm scanned at ≥ 37 weeks gestational age (r^2=0.54, p<0.0001); C: age-matched infants born full-term (r^2 = 0.53; p<0.0001). Each dot is a bundle. D-F: Bootstrap distributions of correlation differences between groups: D: preterm infants scanned shortly after birth vs. full-term infants; E: preterm infants scanned at birth vs. preterm infants scanned at term-equivalent age; F: preterm infants scanned at term-equivalent age vs. full-term infants. The vertical red and green lines indicate 95% confidence intervals (CIs), blue line indicates mean, purple line indicates 0. Zero fell outside the 95% CIs in all comparisons. Abbreviations: AF: Arcuate Fasciculus, ATR: Anterior Thalamic Radiation], CC: Cingulum Cingulate, CS: Cortico-Spinal Tract, FcMa: Forceps Major, FcMi: Forceps Minor, IFO: Inferior Frontal Occipital Fasciculus, ILF: Inferior Longitudinal Fasciculus, MLF: Middle Longitudinal Fasciculus, OR: Optic Radiation, SLF: Superior Longitudinal Fasciculus, UNC: Uncinate Fasciculus, VOF: Ventral Occipital Fasciculus, pARC: Posterior Arcuate Fasciculus, L=left, R=right.

Further comparisons between the three groups revealed a few additional interesting patterns. First, bundles show an overall similar order of development across the age groups: the corticospinal tract (CS) exhibits highest T1w/T2w in both white and gray in each group, while the posterior arcuate fasciculus (pARC) shows consistently low T1w/T2w, with the other bundles falling in between. Across the groups, the cortical targets of the ATR have lower T1w/T2w and the cortical targets of the VOF have higher T1w/T2w than expected based on their white matter T1w/T2w. Second, there are differences in the degree to which bilateral bundles show similar T1w/T2w values in gray matter across the age group: bilateral bundles are more dissimilar at the preterm infants first scan compared to their second scan (group difference in delta of T1w/T2w across hemispheres: p=0.0002, paired t-test), with the full-term infants falling in between.

Discussion

In this study, we examined the association between T1w/T2w of white matter bundles and their corresponding cortical targets in a large-scale infant dataset provided by the dHCP. Our analyses revealed five key findings: (i) T1w/T2w of white matter bundles is positively correlated with T1w/T2w of their respective cortical targets across bundles; (ii) the rate of change (slope) of T1w/T2w is also correlated between white and gray matter, and white matter shows steeper slopes; (iii) there are significant inter-individual differences in T1w/T2w coupling across tissues and (iv) a higher degree of T1w/T2w coupling is associated with better motor skills at 17-25 months of age; (v) the T1w/T2w coupling is lower shortly after preterm compared to full-term birth, yet by term-equivalent age, infants born prematurely show higher correlations than their full-term peers. Overall, these results suggest that white and gray matter are developing in concert during early infancy. .

Our findings relate to prior work linking other gray and white matter properties in different developmental populations. First, during childhood and adolescence (ages 5-23), the maturation of white matter bundles, assessed as the mean diffusivity along the bundles, is closely linked to the maturation of their cortical endpoints. That is, regions in which cortex is developing earlier are connected to earlier developing white matter bundles, while bundles connected to later-developing cortical areas mature later[83]. Further evidence for white and gray matter coupling comes from studies relating white matter properties to cortical thickness and cortical expansion. For example, network-based analyses showed that the white matter connectome architecture impacts cortical thinning in childhood[84]. Cortical thickness has also been shown to correlate positively with fractional anisotropy in connected white matter tracts during childhood[85] and from childhood to adulthood[86]. Further, during childhood, the expansion of cortical surface area parallels increases in the number and maturation of white matter connections terminating in that cortex[87,88]. Studies linking gray and white matter properties during infancy are limited to date, however research showed that white matter connectivity is more strongly impacted by a cortical region's cytoarchitecture than by its functional properties across infancy, childhood, and adulthood[89,90]. Nonetheless, in adults, training-induced changes in functional properties of cortex have also been shown to be associated with white matter changes. For example, motor training of the non-dominant hand induces increased fMRI activation alongside cortical thickening as well as increases in white matter fractional anisotropy in the corresponding bundle[91,92]. Moreover, white matter connectivity, in combination with cortical microstructure, can be used to predict the functional organization of cortex in adulthood[93]. While not specific to changes in myelin, these studies across different developmental populations underscore the importance of conjointly evaluating white and gray matter tissue properties.

Here we find that T1w/T2w development is tightly linked between white matter bundles and their corresponding cortical targets. This observation is most readily accounted for by the theory of activity-dependent myelination[25,94]: According to this theory, active neurons send trophic signals (e.g., glutamatergic release, ATP signaling) along their axons that promote oligodendrocyte differentiation both within the cortex and along white matter projections, such that increased neuronal firing can increase myelination in both compartments[95–98] (for review see[99]). Two additional mechanisms could further contribute to the observed T1w/T2w

coupling: 1) Coordinated genetic regulation might drive myelination of white and gray matter. After all, similar genetic programs direct the proliferation, migration, and differentiation of oligodendrocyte precursor cells (OPCs) in both cortex and white matter[69,100]. 2) Common metabolic and microenvironmental factors may contribute to the observed coupling in myelin development. Both cortical and white matter myelination are energy-demanding processes that depend on a supply of lipids and other metabolic substrates[18] (for review see [101] As such, the local availability of these resources, coupled with support from glial cells like astrocytes could concurrently influence myelination in both tissues[102,103] (for review see[104]).

By simultaneously evaluating changes in both white and gray matter T1w/T2w during early infancy, we had the opportunity to directly compare their growth rates. While the mean T1w/T2w was generally higher in cortex, the slope of T1w/T2w development was steeper in the white matter in the evaluated neonates. These findings can be corroborated when integrating previous research using quantitative MRI metrics such as R1 that are directly comparable across studies. First, across studies, newborn R1 values reported in the white matter (range: 0.4 - 0.6s^{-1})[5] are generally lower than R1 values reported for cortex (range: 0.5 - 0.8s^{-1})[4], suggesting that cortex is more heavily myelinated at birth. Further, across studies, R1 growth rates reported for white matter (approximate R1 increase of 0.026s^{-1}/month)[5], exceed R1 growth rates reported for cortex (approximate R1 increase of 0.015s^{-1}/month))[4] during the first 6 months of life, suggesting that white matter myelin content increases 2x faster during early infancy than cortical myelin content. Although these comparisons across studies provide evidence for a faster rate of white than gray matter myelination in infants, here we could expand upon this by directly comparing developmental rates across both tissues within the same individuals.

Interestingly, we find that inter-individual differences in the T1w/T2w coupling across tissues explains later life motor outcomes. Multiple studies have linked increased myelination of either white or gray matter to motor performance in humans[99,105] (for reviews see[106,107]) and other species such as mice[68,69,96,108–110]. Our findings complement this literature by showing that it may not only be the absolute amount of myelin that impacts motor performance, but also the degree of synchrony in myelination across white matter bundles and their corresponding gray matter targets. Nonetheless, as the observed impact of white and gray matter synchrony on motor performance is comparatively small in the large sample evaluated here, future work is needed to assess the reproducibility and generalizability of this effect. These future studies could relate T1w/T2w synchrony to behavioral assessments conducted concurrently with MRI measurements, as here we are predicting motor performance at 17-25 months of age from neuroimaging data collected at birth, which is inherently ambitious. In addition to motor performance, we also explored the link between inter-individual differences in T1w/T2w coupling and later life language and cognitive skills, but found no significant relationship. One possible explanation for our findings being restricted to motor performance may be the time at which the behavioral assessments took place (17-25 months of age), as early infancy is characterized by a particularly rapid attainment of key motor milestones. In fact, most fine and gross motor skills - such as grasping, reaching, and postural control - are typically acquired between 6 and 12 months of age, with movement beginning to serve adaptive functions from 3 to 4 months post-term[111]. Accordingly, white matter pathways that support motor skills such as the corticospinal tract (CS), and motor areas in cortex are among the earliest to

myelinate, supporting the early emergence of motor abilities in infants and young children[5,54]. Future studies could explore a link between T1w/T2w coupling and language and cognitive abilities later during development.

In a longitudinal sub-sample, we found that preterm infants show lower correlation of T1w/T2w across gray and white matter than their full-term peers at birth, but higher correlation at term-equivalent age. This suggests that the link between T1w/T2w across tissues is dependent on brain maturity as well as on experience. After all, at birth, the brains of preterm infants had less time to mature compared to their full-term born peers, which could explain the observed reduced T1w/T2w coupling. Indeed, research indicates that preterm birth can alter both the speed and degree of brain myelination, potentially leading to developmental differences when compared to full-term infants[59,112,113] (for review see[114]). At term-equivalent age, age-matched preterm and full-term born infants have had the same amount of time to mature, but preterm born infants have spent more time developing outside the womb and hence likely received more sensory input. As such, the observed increased T1w/T2w coupling in preterm compared to full-term born infants at term-equivalent age is consistent with our proposal that this coupling may be driven by activity-dependent processes. The larger T1w/T2w coupling observed in the preterm infants at term-equivalent age is nonetheless surprising in light of our other finding that increased T1w/T2w coupling at birth improves later behavioral outcomes, as preterm infants often show developmental delays, including in their motor development[115,116]. Future work assessing the precise impact of T1w/T2w coupling at different developmental stages on later-life behavioral outcomes are needed to consolidate these findings. Indeed, when assessing children, a previous study found that combining gray and white matter properties better predicts cognitive abilities than assessing only a single tissue[117].

One limitation of the current study is the reliance on T1w/T2w to assess myelin development in infants. To date, there is no direct histological evidence confirming the relationship between T1w/T2w and myelin content during early life. Most studies aiming to validate T1w/T2w as a marker for myelin have compared it with quantitative MRI metrics for which the link to myelin content is more firmly established. These studies found that while T1w/T2w shows strong test-retest reliability[78] and aligns well with quantitative measures in adult cortex[82,118], it does not align well with quantitative myelin measures in adult white matter[79,80]. This inconsistency is underscored by a recent histological analysis of the corpus callosum[81], which raises further doubts about the validity of using T1w/T2w for conclusions regarding adult white matter myelination. It is important to recognize, however, that the myelin content of infant white matter more closely resembles that of adult cortex than adult white matter, which has been shown by comparing R1 values across tissues from different age groups[59]. Recent findings have supported the use of T1w/T2w for evaluating myelination in infant and children white matter[6,119–122], and previous work[59] demonstrated strong consistency between quantitative R1 and T1w/T2w measures across white matter tracts in a small cohort of newborns. Nonetheless, further research is necessary to fully validate T1w/T2w as a marker for myelin across different age groups and brain regions. This validation is especially crucial considering that large-scale initiatives, such as the dHCP, often acquire T1w and T2w images but not quantitative myelin metrics - forcing a trade-off between sample size and measurement validation.

A second limitation of this study is its reliance on mean T1w/T2w across entire white matter bundles, both cortical target regions and over all cortical endpoints. By reducing each tract to a single weighted average value, we inevitably mask any spatial heterogeneity that may exist along its length. Likewise, computing a single weighted average T1w/T2w value across all cortical endpoints fails to capture localized differences at specific cortical subregions, thereby precluding the detection of fine-grained patterns in cortical myeloarchitecture. This approach may also obscure microstructural variations across different cortical layers, as prior research has shown that T1w/T2w values can vary significantly across cortical depths[22,47,52] (for review see[58]). By averaging across entire bundles or endpoints, our analysis may hence lack sensitivity to localized changes or subtle alterations in myelin content but rather provides a birds-eye view of the link between myelin development across tissues. Future studies employing more granular, regionally, or laminar-resolved T1w/T2w analyses could provide a more nuanced understanding of this relationship.

Overall, our study revealed a tight coupling in the development of T1w/T2w across white and gray matter in the infant brain. Recognizing that gray and white matter myelination unfold in concert compels us to rethink how we evaluate early life brain myelination both in research but also in clinical settings. For infant brain research, our findings promote the use of multimodal imaging paradigms - combining, for example, high-resolution myelin mapping (e.g. with quantitative R1) with diffusion-based tracking of white-matter pathways, so that we capture the coupled trajectories of both gray and white matter myelination. Our results also imply that behavioral or neurodevelopmental assessments targeting sensory, motor, or cognitive milestones could be interpreted in light of this dual process: a given delay in skill acquisition might reflect either cortical immaturity, white matter immaturity, or aberrant coupling of myelination across tissues. Ultimately, acknowledging and testing this gray-white matter myelination synchrony will refine our understanding of early life brain development and the mechanisms that drive the rapid establishment of myelin across the infant brain.

Methods

Data

For this project, we used anatomical and diffusion-weighted newborn data provided by the Developing Human Connectome Project (dHCP) (second data release downloaded from http://www.developingconnectome.org/). The aim of the dHCP is to use magnetic resonance imaging (MRI) to create a dynamic map of human brain connectivity at early stages of brain development[123]. Details on data collection parameters are provided directly by the dHCP (http://www.developingconnectome.org/data-release/second-data-release/release-notes/).
The anatomical and diffusion-weighted data used in this project underwent several preprocessing steps as part of the dHCP pipelines[124,125]. The data encompassed 490 sessions, acquired from 445 individuals, which included all necessary data for the current analyses (diffusion MRI, T1-weighted, and T2-weighted images). As a quality assurance measure, we excluded all sessions that exceeded two standard deviations from the mean with respect to

absolute motion and the number of outlier slices replaced by FSL's eddy tool during the preprocessing stage as in our prior work[59]. Eight additional sessions were excluded following visual inspection due to conspicuous image artifacts or alignment errors. Subsequent to the tractography and bundle identification procedures (detailed in the following sections), we implemented an additional quality assurance step by excluding all sessions where one or more white matter bundles contained 10 or fewer streamlines, as in our prior work[59]. These quality assurance steps ensured the robustness and reliability of the data for further analysis. After quality assurance, we divided the data into two partially overlapping samples: The cross-sectional sample comprised 279 neonates scanned shortly after birth, including both preterm (gestational age < 37 weeks) and full-term infants. Of these, 118 were female. The gestational age at birth ranged from 24.57 to 42.29 weeks (mean ± SD: 38.04 ± 3.73 weeks). Scans were performed between 29.29 and 44.71 weeks post-conceptional age (mean ± SD: 39.57 ± 3.09 weeks), with the time interval between birth and scan ranging from 0 to 16.71 weeks (mean ± SD: 1.54 ± 2.21 weeks). The longitudinal sample consisted of two groups. The first group included 26 preterm infants (8 females) who were scanned twice: once shortly after their preterm birth and again at term-equivalent age. For these infants, the mean gestational age at birth was 32.04 ± 2.97 weeks. The first scan occurred at a mean age of 34.33 ± 1.76 weeks, while the second scan was performed at a mean age of 40.70 ± 1.08 weeks. The second group comprised 26 full-term infants matched 1:1 to the preterm group in terms of sex and age at the second scan. This full-term group included 9 females, with a mean gestational age at birth of 40.04 ± 1.02 weeks and a mean scan age of 40.93 ± 1.44 weeks. For brain-behavioral correlation analyses, we focused on the 215 infants (93 females, 55 infants born preterm) that completed the Bayley-III Scales of Infant and Toddler Development, which was collected between 17 and 25 months of age (mean ± SD: 19.15 ± 1.39 months).

Tractography

Diffusion MRI tractography was conducted using MRtrix[126], as in our earlier work[59]. Voxel-wise fiber orientation distributions (FODs) were calculated with constrained spherical deconvolution (CSD) and the Dhollander algorithm was used[127] to estimate three-tissue response functions. Because of the generally lower FA in newborn brains, the FA threshold was set to 0.1. We then computed FODs with multi-shell multi-tissue CSD[128] separately for the white matter and the CSF. The gray matter was not modeled separately, as the b-values between white and gray matter are not sufficiently different to allow a clean separation of the signals in newborns. Finally, we performed multi-tissue informed log-domain intensity normalization and generated a whole brain white matter connectome for each session. Tractography was optimized using the tissue segmentation from the anatomical MRI data (anatomically constrained tractography, ACT[129]), which is particularly useful when gray and white matter cannot be separated in the FODs. For each connectome, we used probabilistic fiber tracking with the following parameters: number of streamlines: 2 million, algorithm: IFOD1, step size: 0.2 mm, minimum length: 4 mm, maximum length: 200 mm, FOD amplitude stopping criterion: 0.05, maximum angle: 15 deg. Seeds for tractography were randomly placed within the gray/white matter interface (from anatomical tissue segmentation), which enabled us to ensure that all streamlines reach the gray matter, which was critical for determining each bundle's cortical terminations.

Bundle identification with pyBabyAFQ

To assess tissue development across bundles and at their cortical targets in a large sample, it is important to identify the bundles systematically and automatically within the native brain space of each individual infant. Automated tools developed for the identification of fiber bundles in individuals are traditionally designed for adult data[130–133] and may not be suitable for the analysis of infant data. In our previous research, we introduced babyAFQ[5,59], an automated fiber quantification tool specifically designed to identify fiber bundles in the infant brain. BabyAFQ is available both for MATLAB[5] and for Python[59] and here we used the Python implementation as it more readily lends itself for scalable deployment. Importantly, babyAFQ is fully integrated into the pyAFQ software package[133], so that additional tools for plotting, bundle profile evaluation, and statistical analysis (e.g., AFQ-insight, https://tractometry.org/AFQ-Insight,[134]) can be applied after bundle identification. As described previously[5], babyAFQ identifies bundles by using sets of anatomical ROIs that serve as waypoints for each bundle. The way-point ROIs were defined in a newborn template brain[135] and are converted from this template space to the native brain space of each individual infant. In cases where a streamline crosses the waypoints for multiple bundles, a probabilistic atlas is applied to assess which bundle is the better fit; this probabilistic atlas is also converted from the newborn template space to the brain space of each individual infant. Prior to this work, babyAFQ identified 24 white matter bundles in individual infant's native brain space (11 in each hemisphere and 2 between-hemispheres): the anterior thalamic radiation (ATR), cortico-spinal tract (CS), forceps major (FcMa), forceps minor (FcMi), arcuate fasciculus (AF), uncinate fasciculus (UNC), superior longitudinal fasciculus (SLF), cingulum cingulate (CC), inferior longitudinal fasciculus (ILF), inferior frontal occipital fasciculus (IFOF), middle longitudinal fasciculus (MLF), ventral occipital fasciculus (VOF) and the posterior arcuate fasciculus (pARC). In the current study we added the optic radiation (OR) to babyAFQ and ported pARC and VOF from the matlab version of babyAFQ (Fig. 1). To identify the OR, the central part of the thalamus and the primary visual cortex (V1) served as endpoint ROIs. These ROIs were based on the work of Caffara et al.[136]. An additional way-point ROI was placed in the white matter along the expected OR pathway (between thalamus and V1). All OR ROIs were defined in the same neonate template brain used to identify the other bundles in babyAFQ. For each bundle, we removed streamlines whose trajectories differed by more than four standard deviations from the bundle's median trajectory, for multiple rounds (see [131] for more details). Cloudknot software[137] was used to deploy both tractography (as described above) and bundle identification to the Amazon Web Services (AWS) Batch service.

Assessing T1w/T2w along bundles and at each bundle's cortical targets

After identifying the bundles with pyBabyAFQ, we evaluated T1w/T2w along their length. For this, each bundle was divided into 100 nodes, and a weighted average of T1w/T2w was computed at each node. In this weighted average, the contribution of a particular streamline depends on the Mahalanobis distance of that streamline to the core of the bundle (the median xyz position of that node). That is, streamlines that are closer to the core of the bundle are weighted more heavily than streamlines that are further away from the core. This is customary in the AFQ method and has two important advantages: (i) streamlines closer to the core are more likely to be accurately assigned and less influenced by partial volume effects

and therefore provide a cleaner measure of the bundle's properties, and (ii) the weighting counteracts the effects of bundle volume on the generated bundle profiles. Importantly, in order to ensure that partial voluming between gray and white matter does not contribute to any observed coupling of T1w/T2w across tissues, the first and last 5 nodes, i.e. the superficial white matter underneath cortex, was excluded from all analyses.

To assess T1w/T2w in the cortical targets of each bundle, first we mapped the endpoints of each streamline of each bundle at the gray-white matter interface, using the tckmap function provided by MRtrix (see Supplementary Figure S3). Subsequently, the resulting endpoint density maps were projected onto the cortical surface using FreeSurfer. For association and inter-hemispheric bundles, which travel from cortex to cortex, this resulted in two cortical areas with endpoints for a given bundle. To distinguish these two cortical areas, the label file (*_desc-drawem_space-T2w_dparc.dlabel.gii)* provided by the dHCP was used to define boundaries, so that the origin and termination areas of each bundle could be analysed individually. Notably, we also included three projection bundles (the anterior thalamic radiation, the cortico-spinal tract, and the optic radiation) which only have a single cortical termination area.

The cortical myelin maps provided by the dHCP were employed to calculate T1w/T2w for every cortical voxel that contains an endpoint density > 0.0001. We then calculated a weighted average across all voxels that contained endpoints for a given bundle, such that voxels with relatively more endpoints also contributed more strongly to the T1w/T2w for that bundle's cortical terminations. This systematic approach enabled the evaluation of both the T1w/T2w along bundles and the cortical T1w/T2w for the target regions of these bundles, facilitating further analysis and investigation.

Modeling T1w/T2w development in cortex and white matter bundles

Next, we related T1w/T2w measured along white matter bundles and their corresponding cortical targets. First, we examined the relationship between mean T1w/T2w in white and gray matter across bundles using the Pearson's correlation coefficient (r) (Fig. 2A). To illustrate inter-individual variability, we also performed subject-wise Pearson correlations and identified three representative cases showing low, intermediate and high correlation values (Fig. 2B-D).

As we found large inter-individual differences in the correlation of T1w/T2w across tissues, next we tested if these inter-individual differences have behavioral consequences. For this, we used a subsample of 215 infants which also completed the Bayley Scales of Infant and Toddler Development, Third Edition (Bayley-III[138]), a standardized tool designed to evaluate development functioning in children from 1 to 42 months of age. We examined three behavioral domains (cognition, language and motor) by taking the sum of raw scores within each respective Bayley-III subscale and related these behavioral outcomes to the correlation of T1w/T2w across white and gray matter at birth (Fig. 3). In addition, we also tested if T1w/T2w measured in each tissue separately relates to later behavioral outcomes (Supplementary Fig. S1). Infants whose performance on a given behavioral domain was 2 standard deviations below the mean were excluded to ensure only data from compliant infants was used for the analyses. Pearson correlations were used to assess associations,

and the coefficient of determination (r^2) was reported for each model. Bonferroni correction was applied.

To further characterize developmental trajectories, we computed T1w/T2w developmental slopes for each bundle and their cortical terminations by relating T1w/T2w to gestational age at scan (in weeks) (model: T1w/T2w ~ 1 + scan age, Fig. 4A-C, Supplementary Fig. S2). Paired t-tests were conducted to assess differences in slopes between tissue types. To evaluate model fits, the Akaike Information Criterion (AIC) was employed. Pearson correlations were employed to test for a relationship between developmental slopes of white matter bundles and their respective cortical targets (Fig. 4D).

To examine the impact of preterm birth and postnatal experience on the correlation of T1w/T2w across tissues, we compared three groups in a small longitudinal sub-sample: (i) preterm infants scanned shortly after birth, (ii) the same preterm infants scanned again at a scan age ≥ 37 weeks, and (iii) full-term infants individually matched to the preterm infants second scan on sex and scan age. For each group, we computed the mean T1w/T2w values in white matter bundles and corresponding cortical targets, and assessed their linear relationship using Pearson's correlation (Fig. 5A-C). To test if the correlation of T1w/T2w across tissues differs between the groups we employed a nonparametric bootstrap procedure[139]. For each group, we generated 1,000 bootstrap samples by drawing, with replacement, n = 26 observations and computed the correlation of T1w/T2w across tissues in each sample. To compare correlations across the three groups, we examined the nonparametric bootstrap distribution of their pairwise differences in r^2, assessing whether zero lay within or outside the central 95% of the interval, which defined the confidence intervals (Fig. 5D-F). When 0 fell outside the confidence intervals, this was interpreted as a significant group difference.

Data, Materials and Software Availability

The data used in the current study were provided by the Developing Human Connectome Project (dHCP[123]) and can be downloaded through their website (http://www.developingconnectome.org/). The data were analyzed using open-source software, including MRtrix[126,140] and pyBabyAFQ, which we shared as a component of pyAFQ (https://yeatmanlab.github.io/pyAFQ,[133]). Code that implemented the tractography pipeline, example code to perform bundle identification with pyBabyAFQ, and code used to generate the main figures of this manuscript are also made available on GitHub (https://github.com/EduNeuroLab).

Acknowledgements

This research was supported by This work was supported by European Research Council Starting Grant 101161197 WRAPPED, by the Deutsche Forschungsgemeinschaft (DFG, German Research Foundation) - project number 222641018 - SFB/TRR 135 TP C10, and The

Adaptive Mind (TAM), funded through the Excellence Program of the Hessian Ministry of Higher Education, Science, Research and Art. This research was further supported by National Institutes of Health grants MH121868, MH121867, and R01EB027585, as well as by National Science Foundation grant 1934292. Open-source software development was also supported by the Chan Zuckerberg Initiative's Essential Open Source Software for Science program, the Alfred P. Sloan Foundation and the Gordon & Betty Moore Foundation. JK was supported through the NSF Graduate Research Fellowship DGE-2140004. Cloud computing resources were supported by the Amazon Web Services Research Credits Program. Data were provided by the developing Human Connectome Project (KCL-Imperial-Oxford Consortium), funded by the European Research Council under the European Union Seventh Framework Programme (FP/2007-2013), ERC Grant Agreement No. 319456. We sincerely thank the families who generously participated in this study.

Author contributions

MG and AR designed the study; SZ, MG, JK, AR, KC and AO contributed code for data analysis; SZ downloaded, processed, and analysed the data; SZ and MG wrote the manuscript. All authors read and provided feedback on the manuscript.

References

1. Knickmeyer, R. C. *et al.* A Structural MRI Study of Human Brain Development from Birth to 2 Years. *J. Neurosci.* **28**, 12176–12182 (2008).
2. Gilmore, J. H., Knickmeyer, R. C. & Gao, W. Imaging structural and functional brain development in early childhood. *Nat. Rev. Neurosci.* **19**, 123–137 (2018).
3. Deoni, S. C. L. *et al.* Mapping Infant Brain Myelination with Magnetic Resonance Imaging. *J. Neurosci.* **31**, 784–791 (2011).
4. Natu, V. S. *et al.* Infants' cortex undergoes microstructural growth coupled with myelination during development. *Commun. Biol.* **4**, 1191 (2021).
5. Grotheer, M. *et al.* White matter myelination during early infancy is linked to spatial gradients and myelin content at birth. *Nat. Commun.* **13**, 997 (2022).
6. Filimonova, E., Amelina, E., Sazonova, A., Zaitsev, B. & Rzaev, J. Assessment of normal myelination in infants and young children using the T1w/T2w mapping technique. *Front. Neurosci.* **17**, 1102691 (2023).
7. Stiles, J. & Jernigan, T. L. The Basics of Brain Development. *Neuropsychol. Rev.* **20**,

327–348 (2010).

8. Lebel, C. & Deoni, S. The development of brain white matter microstructure. *NeuroImage* **182**, 207–218 (2018).
9. Dubois, J. *et al.* The early development of brain white matter: A review of imaging studies in fetuses, newborns and infants. *Neuroscience* **276**, 48–71 (2014).
10. Khanbabaei, M. *et al.* Precocious myelination in a mouse model of autism. *Transl. Psychiatry* **9**, 251 (2019).
11. De Faria, O. *et al.* Periods of synchronized myelin changes shape brain function and plasticity. *Nat. Neurosci.* **24**, 1508–1521 (2021).
12. Fields, R. D. White matter in learning, cognition and psychiatric disorders. *Trends Neurosci.* **31**, 361–370 (2008).
13. Stadelmann, C., Timmler, S., Barrantes-Freer, A. & Simons, M. Myelin in the Central Nervous System: Structure, Function, and Pathology. *Physiol. Rev.* **99**, 1381–1431 (2019).
14. Chen, B. *et al.* Cortical myelination in toddlers and preschoolers with autism spectrum disorder. *Dev. Neurobiol.* **82**, 261–274 (2022).
15. Khelfaoui, H., Ibaceta-Gonzalez, C. & Angulo, M. C. Functional myelin in cognition and neurodevelopmental disorders. *Cell. Mol. Life Sci.* **81**, 181 (2024).
16. Frankenhaeuser, B. Saltatory conduction in myelinated fibres. **J. Physiol.**, 118 (1954).
17. Fruttiger, M., Montag, D., Schachner, M. & Martini, R. Crucial Role for the Myelin‐associated Glycoprotein in the Maintenance of Axon‐Myelin Integrity. *Eur. J. Neurosci.* **7**, 511–515 (1995).
18. Harris, J. J. & Attwell, D. The Energetics of CNS White Matter. *J. Neurosci.* **32**, 356–371 (2012).
19. Simons, M. & Nave, K.-A. Oligodendrocytes: Myelination and Axonal Support. *Cold Spring Harb. Perspect. Biol.* **8**, a020479 (2016).
20. O'Brien, J. S. & Sampson, E. L. Lipid composition of the normal human brain: gray

matter, white matter, and myelin. *J. Lipid Res.* **6**, 537–544 (1965).

21. Osetrova, M. *et al.* Lipidome atlas of the adult human brain. *Nat. Commun.* **15**, 4455 (2024).

22. Glasser, M. F. & Van Essen, D. C. Mapping Human Cortical Areas *In Vivo* Based on Myelin Content as Revealed by T1- and T2-Weighted MRI. *J. Neurosci.* **31**, 11597–11616 (2011).

23. Tomassy, G. S. *et al.* Distinct Profiles of Myelin Distribution Along Single Axons of Pyramidal Neurons in the Neocortex. *Science* **344**, 319–324 (2014).

24. Nieuwenhuys, R. The myeloarchitectonic studies on the human cerebral cortex of the Vogt–Vogt school, and their significance for the interpretation of functional neuroimaging data. *Brain Struct. Funct.* **218**, 303–352 (2013).

25. Fields, R. D. A new mechanism of nervous system plasticity: activity-dependent myelination. *Nat. Rev. Neurosci.* **16**, 756–767 (2015).

26. Turner, R. Myelin and Modeling: Bootstrapping Cortical Microcircuits. *Front. Neural Circuits* **13**, 34 (2019).

27. Timmler, S. & Simons, M. Grey matter myelination. *Glia* **67**, 2063–2070 (2019).

28. Micheva, K. D. *et al.* A large fraction of neocortical myelin ensheathes axons of local inhibitory neurons. *eLife* **5**, e15784 (2016).

29. Snaidero, N. *et al.* Myelin replacement triggered by single-cell demyelination in mouse cortex. *Nat. Commun.* **11**, 4901 (2020).

30. Orthmann-Murphy, J. *et al.* Remyelination alters the pattern of myelin in the cerebral cortex. *eLife* **9**, e56621 (2020).

31. Takesian, A. E. & Hensch, T. K. Balancing Plasticity/Stability Across Brain Development. in *Progress in Brain Research* vol. 207 3–34 (Elsevier, 2013).

32. Budd, J. M. L. *et al.* Neocortical Axon Arbors Trade-off Material and Conduction Delay Conservation. *PLoS Comput. Biol.* **6**, e1000711 (2010).

33. Kapfhammer, J. & Schwab, M. E. Inverse patterns of myelination and GAP-43 expression in the adult CNS: Neurite growth inhibitors as regulators of neuronal plasticity?

J. Comp. Neurol. **340**, 194–206 (1994).

34. McKerracher, L. *et al.* Identification of myelin-associated glycoprotein as a major myelin-derived inhibitor of neurite growth. *Neuron* **13**, 805–811 (1994).

35. McGee, A. W. & Strittmatter, S. M. The Nogo-66 receptor: focusing myelin inhibition of axon regeneration. *Trends Neurosci.* **26**, 193–198 (2003).

36. McGee, A. W., Yang, Y., Fischer, Q. S., Daw, N. W. & Strittmatter, S. M. Experience-Driven Plasticity of Visual Cortex Limited by Myelin and Nogo Receptor. *Science* **309**, 2222–2226 (2005).

37. Filbin, M. T. Myelin-associated inhibitors of axonal regeneration in the adult mammalian CNS. *Nat. Rev. Neurosci.* **4**, 703–713 (2003).

38. Yakovlev, P., Lecours, A., Minkowski, A. & Davis, F. Regional develoment of the brain in early life. (1967).

39. Poduslo, S. E. & Jang, Y. Myelin development in infant brain. *Neurochem. Res.* **9**, 1615–1626 (1984).

40. Brody, B. A., Kinney, H. C., Kloman, A. S. & Gilles, F. H. Sequence of Central Nervous System Myelination in Human Infancy. I. An Autopsy Study of Myelination: *J. Neuropathol. Exp. Neurol.* **46**, 283–301 (1987).

41. Kinney, H. C., Ann Brody, B., Kloman, A. S. & Gilles, F. H. Sequence of Central Nervous System Myelination in Human Infancy. II. Patterns of Myelination in Autopsied Infants: *J. Neuropathol. Exp. Neurol.* **47**, 217–234 (1988).

42. Barkovich, A. J. & Kjos, B. O. Normal postnatal development of the corpus callosum as demonstrated by MR imaging. **American Journal of Neuroradiology**, 487–491 (1988).

43. Deoni, S. C. L., Dean, D. C., O'Muircheartaigh, J., Dirks, H. & Jerskey, B. A. Investigating white matter development in infancy and early childhood using myelin water faction and relaxation time mapping. *NeuroImage* **63**, 1038–1053 (2012).

44. Lebel, C. *et al.* Diffusion tensor imaging of white matter tract evolution over the lifespan. *NeuroImage* **60**, 340–352 (2012).

45. Groeschel, S. *et al.* Assessing White Matter Microstructure in Brain Regions with Different Myelin Architecture Using MRI. *PLOS ONE* **11**, e0167274 (2016).

46. Hopf, A. Über die Verteilung myeloarchitektonischer Merkmale in der Stirnhirnrinde beim Menschen. *J Hirnforsch* **2**, 311–333 (1956).

47. Hopf, A. & Vitzthum, H. G. Über die Verteilung myeloarchitektonischer Merkmale in der Scheitellappenrinde beim Menschen. *J Hirnforsch* **3**, 83–104 (1957).

48. Sanides, F. Die Stirnhirnrinde. in *Die Architektonik des Menschlichen Stirnhirns* vol. 98 65–176 (Springer Berlin Heidelberg, Berlin, Heidelberg, 1962).

49. Bock, N. A., Kocharyan, A., Liu, J. V. & Silva, A. C. Visualizing the entire cortical myelination pattern in marmosets with magnetic resonance imaging. *J. Neurosci. Methods* **185**, 15–22 (2009).

50. Huntenburg, J. M. *et al.* A Systematic Relationship Between Functional Connectivity and Intracortical Myelin in the Human Cerebral Cortex. *Cereb. Cortex* **27**, 981–997 (2017).

51. Buyanova, I. S. & Arsalidou, M. Cerebral White Matter Myelination and Relations to Age, Gender, and Cognition: A Selective Review. *Front. Hum. Neurosci.* **15**, 662031 (2021).

52. Flechsig, P. *Die Myelogenetische Gliederung Der Leitungsbahnen Des Linsenkerns Beim Menschen*. vol. 73 (Berichte über die Verhandlungen der Sächsischen Akademie der Wissenschaften zu Leipzig: Mathematisch-Physische Klasse, 1921).

53. Collins, C. E., Airey, D. C., Young, N. A., Leitch, D. B. & Kaas, J. H. Neuron densities vary across and within cortical areas in primates. *Proc. Natl. Acad. Sci.* **107**, 15927–15932 (2010).

54. Deoni, S. C. L., Dean, D. C., Remer, J., Dirks, H. & O'Muircheartaigh, J. Cortical maturation and myelination in healthy toddlers and young children. *NeuroImage* **115**, 147–161 (2015).

55. Miller, D. J. *et al.* Prolonged myelination in human neocortical evolution. *Proc. Natl. Acad. Sci.* **109**, 16480–16485 (2012).

56. Glasser, M. F. *et al.* A multi-modal parcellation of human cerebral cortex. *Nature* **536**, 171–178 (2016).

57. Lebenberg, J. *et al.* Mapping the asynchrony of cortical maturation in the infant brain: A MRI multi-parametric clustering approach. *NeuroImage* **185**, 641–653 (2019).

58. Glasser, M. F., Goyal, M. S., Preuss, T. M., Raichle, M. E. & Van Essen, D. C. Trends and properties of human cerebral cortex: Correlations with cortical myelin content. *NeuroImage* **93**, 165–175 (2014).

59. Grotheer, M. *et al.* Human white matter myelinates faster in utero than ex utero. *Proc. Natl. Acad. Sci.* **120**, e2303491120 (2023).

60. Dubois, J., Adibpour, P., Poupon, C., Hertz-Pannier, L. & Dehaene-Lambertz, G. MRI and M/EEG studies of the White Matter Development in Human Fetuses and Infants: Review and Opinion. *Brain Plast.* **2**, 49–69 (2016).

61. Rosenke, M., Van Hoof, R., Van Den Hurk, J., Grill-Spector, K. & Goebel, R. A Probabilistic Functional Atlas of Human Occipito-Temporal Visual Cortex. *Cereb. Cortex* **31**, 603–619 (2021).

62. Sydnor, V. J. *et al.* Neurodevelopment of the association cortices: Patterns, mechanisms, and implications for psychopathology. *Neuron* **109**, 2820–2846 (2021).

63. Barres, B. A. & Raff, M. C. Proliferation of oligodendrocyte precursor cells depends on electrical activity in axons. *Nature* **361**, 258–260 (1993).

64. Stevens, B., Porta, S., Haak, L. L., Gallo, V. & Fields, R. D. Adenosine. *Neuron* **36**, 855–868 (2002).

65. Wake, H., Lee, P. R. & Fields, R. D. Control of Local Protein Synthesis and Initial Events in Myelination by Action Potentials. *Science* **333**, 1647–1651 (2011).

66. Monje, M. Myelin Plasticity and Nervous System Function. *Annu. Rev. Neurosci.* **41**, 61–76 (2018).

67. Liu, J. *et al.* Impaired adult myelination in the prefrontal cortex of socially isolated mice. *Nat. Neurosci.* **15**, 1621–1623 (2012).

68. Sampaio-Baptista, C. *et al.* Motor Skill Learning Induces Changes in White Matter

Microstructure and Myelination. *J. Neurosci.* **33**, 19499–19503 (2013).

69. Gibson, E. M. *et al.* Neuronal Activity Promotes Oligodendrogenesis and Adaptive Myelination in the Mammalian Brain. *Science* **344**, 1252304 (2014).

70. Mount, C. W. & Monje, M. Wrapped to Adapt: Experience-Dependent Myelination. *Neuron* **95**, 743–756 (2017).

71. Mezer, A. *et al.* Quantifying the local tissue volume and composition in individual brains with magnetic resonance imaging. *Nat. Med.* **19**, 1667–1672 (2013).

72. Lutti, A., Dick, F., Sereno, M. I. & Weiskopf, N. Using high-resolution quantitative mapping of R1 as an index of cortical myelination. *NeuroImage* **93**, 176–188 (2014).

73. Edwards, L. J., Kirilina, E., Mohammadi, S. & Weiskopf, N. Microstructural imaging of human neocortex in vivo. *NeuroImage* **182**, 184–206 (2018).

74. Dubois, J. *et al.* MRI of the Neonatal Brain: A Review of Methodological Challenges and Neuroscientific Advances. *J. Magn. Reson. Imaging* **53**, 1318–1343 (2021).

75. Stüber, C. *et al.* Myelin and iron concentration in the human brain: A quantitative study of MRI contrast. *NeuroImage* **93**, 95–106 (2014).

76. Laule, C. & Moore, G. R. W. Myelin water imaging to detect demyelination and remyelination and its validation in pathology. *Brain Pathol.* **28**, 750–764 (2018).

77. Thompson, G. J. *et al.* Histological Validation of Multi-Echo Gradient Echo (MGRE)-Derived Myelin Water Fraction (MWF) at 9.4 T and the Influence of Orientation on Quantification. *NMR Biomed.* **38**, e5303 (2025).

78. Arshad, M., Stanley, J. A. & Raz, N. Test–retest reliability and concurrent validity of in vivo myelin content indices: Myelin water fraction and calibrated T_1 w/T_2 w image ratio. *Hum. Brain Mapp.* **38**, 1780–1790 (2017).

79. Uddin, M. N., Figley, T. D., Marrie, R. A., Figley, C. R., & for the CCOMS Study Group. Can T_1 w/ T_2 w ratio be used as a myelin-specific measure in subcortical structures? Comparisons between FSE-based T_1 w/ T_2 w ratios, GRASE-based T_1 w/ T_2 w ratios and multi-echo GRASE-based myelin water fractions. *NMR Biomed.* **31**, e3868 (2018).

80. Uddin, Md. N., Figley, T. D., Solar, K. G., Shatil, A. S. & Figley, C. R. Comparisons between multi-component myelin water fraction, T1w/T2w ratio, and diffusion tensor imaging measures in healthy human brain structures. *Sci. Rep.* **9**, 2500 (2019).

81. Sandrone, S. *et al.* Mapping myelin in white matter with T1-weighted/T2-weighted maps: discrepancy with histology and other myelin MRI measures. *Brain Struct. Funct.* **228**, 525–535 (2023).

82. Shams, Z., Norris, D. G. & Marques, J. P. A comparison of in vivo MRI based cortical myelin mapping using T1w/T2w and R1 mapping at 3T. *PLOS ONE* **14**, e0218089 (2019).

83. Luo, A. C. *et al.* Two Axes of White Matter Development. Preprint at https://doi.org/10.1101/2025.03.19.644049 (2025).

84. Liang, X. *et al.* Structural connectome architecture shapes the maturation of cortical morphology from childhood to adolescence. *Nat. Commun.* **15**, 784 (2024).

85. Wu, M. *et al.* Development of superficial white matter and its structural interplay with cortical gray matter in children and adolescents. *Hum. Brain Mapp.* **35**, 2806–2816 (2014).

86. Kochunov, P. *et al.* Fractional anisotropy of cerebral white matter and thickness of cortical gray matter across the lifespan. *NeuroImage* **58**, 41–49 (2011).

87. Raznahan, A. *et al.* Patterns of Coordinated Anatomical Change in Human Cortical Development: A Longitudinal Neuroimaging Study of Maturational Coupling. *Neuron* **72**, 873–884 (2011).

88. Cafiero, R., Brauer, J., Anwander, A. & Friederici, A. D. The Concurrence of Cortical Surface Area Expansion and White Matter Myelination in Human Brain Development. *Cereb. Cortex* **29**, 827–837 (2019).

89. Kubota, E. *et al.* White matter connections of high-level visual areas predict cytoarchitecture better than category-selectivity in childhood, but not adulthood. *Cereb. Cortex* **33**, 2485–2506 (2023).

90. Kubota, E. *et al.* White matter connections of human ventral temporal cortex are organized by cytoarchitecture, eccentricity and category-selectivity from birth. *Nat. Hum.*

Behav. **9**, 955–970 (2025).

91. Sale, M. V. *et al.* Brain changes following four weeks of unimanual motor training: Evidence from behavior, neural stimulation, cortical thickness, and functional MRI: Widespread Training-Induced Changes in the Human Brain. *Hum. Brain Mapp.* **38**, 4773–4787 (2017).

92. Reid, L. B., Sale, M. V., Cunnington, R., Mattingley, J. B. & Rose, S. E. Brain changes following four weeks of unimanual motor training: Evidence from fMRI-guided diffusion MRI tractography. *Hum. Brain Mapp.* **38**, 4302–4312 (2017).

93. Grotheer, M., Yeatman, J. & Grill-Spector, K. White matter fascicles and cortical microstructure predict reading-related responses in human ventral temporal cortex. *NeuroImage* **227**, 117669 (2021).

94. Noori, R. *et al.* Activity-dependent myelination: A glial mechanism of oscillatory self-organization in large-scale brain networks. *Proc. Natl. Acad. Sci.* **117**, 13227–13237 (2020).

95. Okuda, H. *et al.* Environmental enrichment stimulates progenitor cell proliferation in the amygdala. *J. Neurosci. Res.* **87**, 3546–3553 (2009).

96. McKenzie, I. A. *et al.* Motor skill learning requires active central myelination. *Science* **346**, 318–322 (2014).

97. Hines, J. H., Ravanelli, A. M., Schwindt, R., Scott, E. K. & Appel, B. Neuronal activity biases axon selection for myelination in vivo. *Nat. Neurosci.* **18**, 683–689 (2015).

98. Wake, H. *et al.* Nonsynaptic junctions on myelinating glia promote preferential myelination of electrically active axons. *Nat. Commun.* **6**, 7844 (2015).

99. Zatorre, R. J., Fields, R. D. & Johansen-Berg, H. Plasticity in gray and white: neuroimaging changes in brain structure during learning. *Nat. Neurosci.* **15**, 528–536 (2012).

100. Yeung, M. S. Y. *et al.* Dynamics of Oligodendrocyte Generation and Myelination in the Human Brain. *Cell* **159**, 766–774 (2014).

101. Tepavčević, V. Oligodendroglial Energy Metabolism and (re)Myelination. *Life* **11**, 238

(2021).

102. Fünfschilling, U. *et al.* Glycolytic oligodendrocytes maintain myelin and long-term axonal integrity. *Nature* **485**, 517–521 (2012).

103. Saab, A. S. *et al.* Oligodendroglial NMDA Receptors Regulate Glucose Import and Axonal Energy Metabolism. *Neuron* **91**, 119–132 (2016).

104. Nave, K.-A. & Werner, H. B. Myelination of the Nervous System: Mechanisms and Functions. *Annu. Rev. Cell Dev. Biol.* **30**, 503–533 (2014).

105. Scholz, J., Klein, M. C., Behrens, T. E. J. & Johansen-Berg, H. Training induces changes in white-matter architecture. *Nat. Neurosci.* **12**, 1370–1371 (2009).

106. Bechler, M. E., Swire, M. & ffrench-Constant, C. Intrinsic and adaptive myelination—A sequential mechanism for smart wiring in the brain. *Dev. Neurobiol.* **78**, 68–79 (2018).

107. Bloom, M. S., Orthmann-Murphy, J. & Grinspan, J. B. Motor Learning and Physical Exercise in Adaptive Myelination and Remyelination. *ASN Neuro* **14**, 17590914221097510 (2022).

108. Xiao, L. *et al.* Rapid production of new oligodendrocytes is required in the earliest stages of motor-skill learning. *Nat. Neurosci.* **19**, 1210–1217 (2016).

109. Zheng, J., Sun, X., Ma, C., Li, B. & Luo, F. Voluntary wheel running promotes myelination in the motor cortex through Wnt signaling in mice. *Mol. Brain* **12**, 85 (2019).

110. Bacmeister, C. M. *et al.* Motor learning promotes remyelination via new and surviving oligodendrocytes. *Nat. Neurosci.* **23**, 819–831 (2020).

111. Hadders-Algra, M. Neural substrate and clinical significance of general movements: an update. *Dev. Med. Child Neurol.* **60**, 39–46 (2018).

112. Thompson, D. K. *et al.* Characterization of the corpus callosum in very preterm and full-term infants utilizing MRI. *NeuroImage* **55**, 479–490 (2011).

113. Lee, W., Morgan, B. R., Shroff, M. M., Sled, J. G. & Taylor, M. J. The development of regional functional connectivity in preterm infants into early childhood. *Neuroradiology* **55**, 105–111 (2013).

114. Counsell, S. J. & Boardman, J. P. Differential brain growth in the infant born preterm: Current knowledge and future developments from brain imaging. *Semin. Fetal. Neonatal Med.* **10**, 403–410 (2005).

115. Ko, J. & Lim, H. K. Motor Development Comparison between Preterm and Full-Term Infants Using Alberta Infant Motor Scale. *Int. J. Environ. Res. Public. Health* **20**, 3819 (2023).

116. Maggi, E. F., Magalhães, L. C., Campos, A. F. & Bouzada, M. C. F. Preterm children have unfavorable motor, cognitive, and functional performance when compared to term children of preschool age. *J. Pediatr. (Rio J.)* **90**, 377–383 (2014).

117. Michel, L. C., McCormick, E. M. & Kievit, R. A. Grey and white matter metrics demonstrate distinct and complementary prediction of differences in cognitive performance in children: Findings from ABCD (N= 11 876). *J. Neurosci.* e0465232023 (2024) doi:10.1523/JNEUROSCI.0465-23.2023.

118. Moskovich, S., Shtangel, O. & Mezer, A. A. Approximating R_1 and R_2 : A Quantitative Approach to Clinical Weighted MRI. *Hum. Brain Mapp.* **45**, e70102 (2024).

119. Soun, J. E., Liu, M. Z., Cauley, K. A. & Grinband, J. Evaluation of neonatal brain myelination using the T1- and T2-weighted MRI ratio. *J. Magn. Reson. Imaging* **46**, 690–696 (2017).

120. Darki, F., Nyström, P., McAlonan, G., Bölte, S. & Falck-Ytter, T. T1-Weighted/T2-Weighted Ratio Mapping at 5 Months Captures Individual Differences in Behavioral Development and Differentiates Infants at Familial Risk for Autism from Controls. *Cereb. Cortex* **31**, 4068–4077 (2021).

121. Boroshok, A. L. *et al.* Individual differences in T1w/T2w ratio development during childhood. *Dev. Cogn. Neurosci.* **62**, 101270 (2023).

122. Dipnall, L. M. *et al.* Childhood development of brain white matter myelin: a longitudinal T1w/T2w-ratio study. *Brain Struct. Funct.* **229**, 151–159 (2023).

123. Hughes, E. J. *et al.* A dedicated neonatal brain imaging system: A Dedicated

Neonatal Brain Imaging System. *Magn. Reson. Med.* **78**, 794–804 (2017).

124. Bastiani, M. *et al.* Automated processing pipeline for neonatal diffusion MRI in the developing Human Connectome Project. *NeuroImage* **185**, 750–763 (2019).

125. Glasser, M. F. *et al.* The minimal preprocessing pipelines for the Human Connectome Project. *NeuroImage* **80**, 105–124 (2013).

126. Tournier, J.-D. *et al.* MRtrix3: A fast, flexible and open software framework for medical image processing and visualisation. *NeuroImage* **202**, 116137 (2019).

127. Dhollander, T., Raffelt, D. & Connelly, A. Unsupervised 3-tissue response function estimation from single-shell or multi-shell diffusion MR data without a co-registered t1 image. (2016).

128. Jeurissen, B., Tournier, J.-D., Dhollander, T., Connelly, A. & Sijbers, J. Multi-tissue constrained spherical deconvolution for improved analysis of multi-shell diffusion MRI data. *NeuroImage* **103**, 411–426 (2014).

129. Smith, R. E., Tournier, J.-D., Calamante, F. & Connelly, A. Anatomically-constrained tractography: Improved diffusion MRI streamlines tractography through effective use of anatomical information. *NeuroImage* **62**, 1924–1938 (2012).

130. Yendiki, A. Automated probabilistic reconstruction of white-matter pathways in health and disease using an atlas of the underlying anatomy. *Front. Neuroinformatics* **5**, (2011).

131. Yeatman, J. D., Dougherty, R. F., Myall, N. J., Wandell, B. A. & Feldman, H. M. Tract Profiles of White Matter Properties: Automating Fiber-Tract Quantification. *PLoS ONE* **7**, e49790 (2012).

132. Garyfallidis, E. *et al.* Recognition of white matter bundles using local and global streamline-based registration and clustering. *NeuroImage* **170**, 283–295 (2018).

133. Kruper, J. *et al.* Evaluating the Reliability of Human Brain White Matter Tractometry. *Aperture Neuro* **2021**, 25 (2021).

134. Richie-Halford, A., Yeatman, J. D., Simon, N. & Rokem, A. Multidimensional analysis and detection of informative features in human brain white matter. *PLOS Comput. Biol.* **17**, e1009136 (2021).

135. Shi, F. *et al.* Infant Brain Atlases from Neonates to 1- and 2-Year-Olds. *PLoS ONE* **6**, e18746 (2011).

136. Caffarra, S. *et al.* Development of the visual white matter pathways mediates development of electrophysiological responses in visual cortex. *Hum. Brain Mapp.* **42**, 5785–5797 (2021).

137. Richie-Halford, A. & Rokem, A. Cloudknot: A Python Library to Run your Existing Code on AWS Batch. in 8–14 (Austin, Texas, 2018). doi:10.25080/Majora-4af1f417-001.

138. Bayley, N. Bayley Scales of Infant and Toddler Development, Third Edition. https://doi.org/10.1037/t14978-000 (2006).

139. Ohtani, K. Bootstrapping R2 and adjusted R2 in regression analysis. *Econ. Model.* **17**, 473–483 (2000).

140. Tournier, J., Calamante, F. & Connelly, A. MRtrix: Diffusion tractography in crossing fiber regions. *Int. J. Imaging Syst. Technol.* **22**, 53–66 (2012).